Heliyon 10 (2024) e29355

Contents lists available at ScienceDirect

Heliyon

journal homepage: www.cell.com/heliyon

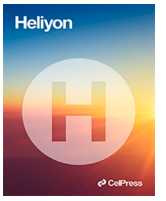

Research article

Fabrication and characterization of new Fe_3O_4@SiO_2@TiO_2-CPTS-HBAP (FST-CH) nanoparticles for photocatalytic degradation and adsorption removal of rhodamine B dye in the aquatic environment

Aysel Cimen [a,*], Ali Bilgic [b], Melike Bayrak [a]

[a] Department of Chemistry, Kamil Ozdag Science Faculty, Karamanoglu Mehmetbey University, 70100, Karaman, Turkey
[b] Vocational School of Technical Sciences, Karamanoglu Mehmetbey University, 70100, Karaman, Turkey

ARTICLE INFO

Keywords:
The photocatalytic degradation
Nanoparticle
Rhodamine B dye (RhB)
Adsorption

ABSTRACT

In this study, **Fe3O4@SiO2@TiO2-CPTS-HBAP** (**FST-CH**) nanoparticle was prepared for the simultaneous adsorption and photocatalytic degradation of aromatic chemical pollutants (Rhodamine B dye) in aqueous solution. ***FST-CH*** nanoparticle was characterized using scanning electron microscopy (SEM), Fourier-transform infrared spectroscopy (FTIR), Energy Dispersive X-Ray (EDX) Fluorescence Spectrometer and X-Ray Diffraction (XRD) spectroscopy. The photocatalytic activity of rhodamine B dye (RhB) was evaluated with a Kerman UV 8/18 vertical roller photoreactor. About 56% of RhB in aqueous medium was adsorbed by ***FST-CH*** nanoparticles with only 45 min of stirring in the dark, and about 77.01% was degraded or converted to other structures under the photoreactor for 120 min. The photocatalytic degradation of RhB (apparent rate constant: 0.0026 mg dm^{-3} min^{-1}) occurred by a pseudo-second order reaction. In addition, the recovery of the prepared magnetic FST-CH nanoparticle by an external magnetic field, exhibiting good magnetic response and reusability, shows that the obtained magnetic ***FST-CH*** nanoparticle is stable and maintains high degradation ratio and catalyst recovery even after four cycles. Thus, the prepared ***FST-CH*** nanoparticle can be highly recommended for its use in potential applications of water decontamination.

1. Introduction

With the rapid rise population of the world, industrialization in countries is increasing rapidly and continues to increase in order to supply the wants of the increasing population. Although the increase in industrialization provides positive benefits to the needs of people, organic substances (paint, medicine, etc.), heavy metals and other wastes released from these industrial establishments are among the pollutants harmful to the environment [1]. Especially organic contaminants are accepted the main concern among water contaminants because they contain a large part of industrial production, have high toxicity, and have poor self-degradation capability [2,3]. Dyes, one of the organic pollutants, are extensively used in growing industrial sectors such as paper, woven, plastic, food, integument, and pharmaceutical corporation, and they release wastewater containing dyes from these sectors to the environment [4]. Owing to their chemical stability, high aromaticity, low biodegradability, carcinogenic, poisonous structure, and widespread

* Corresponding author.
E-mail addresses: ayselcimen42@hotmail.com (A. Cimen), alibilgic100@hotmail.com (A. Bilgic).

https://doi.org/10.1016/j.heliyon.2024.e29355
Received 1 September 2023; Received in revised form 16 February 2024; Accepted 5 April 2024
Available online 6 April 2024

manufacture, these organic dyes are the main environmental pollutants that cause water contamination [5–7]. The amount of dyes released into the water is clearly visible from the water surface, even at very low concentrations. In addition, these dyes poison the water, making it harmful for humans, the environment and living things living near water [6,8].

N-[9-(*ortho*-carboxyphenyl)-6-(diethylamino)-3H-xanthen-3-yli-dene]diethyl ammonium chloride (Rhodamine B (RhB)) is a red organic dye that dissolves extremely well in water [9]. RhB is a dye that is widely used in a variety of sectors, including food, leather, and textiles [10]. However, this highly toxic colorant exhibits behaviors that are mutagenic and carcinogenic to all living things [10, 11]. RhB also creates a threat a serious and permanent threat to aquaus life, especially herbs, as it prevents light from penetrating the water, decreasing photosynthesis and interfering with the environment's normal decontamination processes [10]. RhB must therefore be entirely removed from industrial wastewater in order to prevent the potentially harmful effects caused by its presence in the ecosystem. So far, well-known purification methods such as ion exchange, biological purification, flocculation, membranes, adsorption, coagulation and precipitation have been used to remove organic dyes such as RhB from water [12–14]. However, most of these methods are either inefficient, expensive, time-consuming, or involve too many chemicals [12,15,16]. Also, these traditional methods create secondary pollutants by transferring paint waste from one phase to another [12]. Because of the degradation and full mineralization of permanent dyes, heterogeneous photocatalysis using of semiconductor nanomaterials has recently received considerable interest in the removal of dyes such as RhB [12,17–19].

Advanced oxidative processes have recently been stated to be the best method for decomposing organic matter in water and wastewater [20–22].These processes rely on the production of very reactive radicals, such as hydroxyl groups, which oxidize organic compounds and break them down into innocuous products, like H_2O and CO_2 [22–24]. In recent years, many photocatalytic semiconductor nanomaterials developed with the help of heterogeneous photocatalysts are used as photocatalysts for the degradation of toxic compounds in water [25,26]. Anatase titanium dioxide (TiO_2) is among these catalysts due to its ease of production, low cost, high photoactivity, high chemical and thermal steadiness, non-toxicity and also good electrical conductivity [12,21,22,27]. However, there are various problems with nano- TiO_2 particles suspended in purified water in this treatment process [21]. Due to the nanometric particle size, ultrafiltration was the primary method for recovering TiO_2 from the treated wastewater [21,28]. Another approach is the immobilization of semiconductors' particles on a solid substrate, which may lead to a sharp reduction in a particular surface field and thus decrease the photocatalytic activity [21]. For these reasons, TiO_2 is only appropriate for use in UV light to form electron hole pairs. As an alternative to these disadvantages of TiO_2, especially the use of Fe_3O_4 magnetic photocatalysts (Fe_3O_4 and TiO_2) will be an effective way to solve the difficulty of recovering TiO_2 [29]. Due to its both magnetic and non-toxic properties, iron oxide (Fe_3O_4) is useful as a magnetically sensitive nucleus and is capsulated in a TiO_2 photocatalytic crust [30]. Iron oxide (Fe_3O_4) can cause decomposition and photodecomposition as it can trap electrons. Therefore, a SiO_2 slim stratum is incorporated between the magnetically sensible nucleus Fe_3O_4 and the TiO_2 photocatalytic shell to stabilize the Fe_3O_4 nucleus and decrease the unwanted interaction between the nucleus and the crust [30–32]. To date, this core-layer-shell ($TiO_2/SiO_2@Fe_3O_4$, $Fe_3O_4@SiO_2@TiO_2$, $TiO_2/SiO_2/Fe_3O_4$, etc.) structure has been used in the decomposition of many organic dyes and several biodegradable compounds [33–40]. As a result of the researches, there is no study that affects the functionalization of the $Fe_3O_4@SiO_2@TiO_2$ surfaces with the

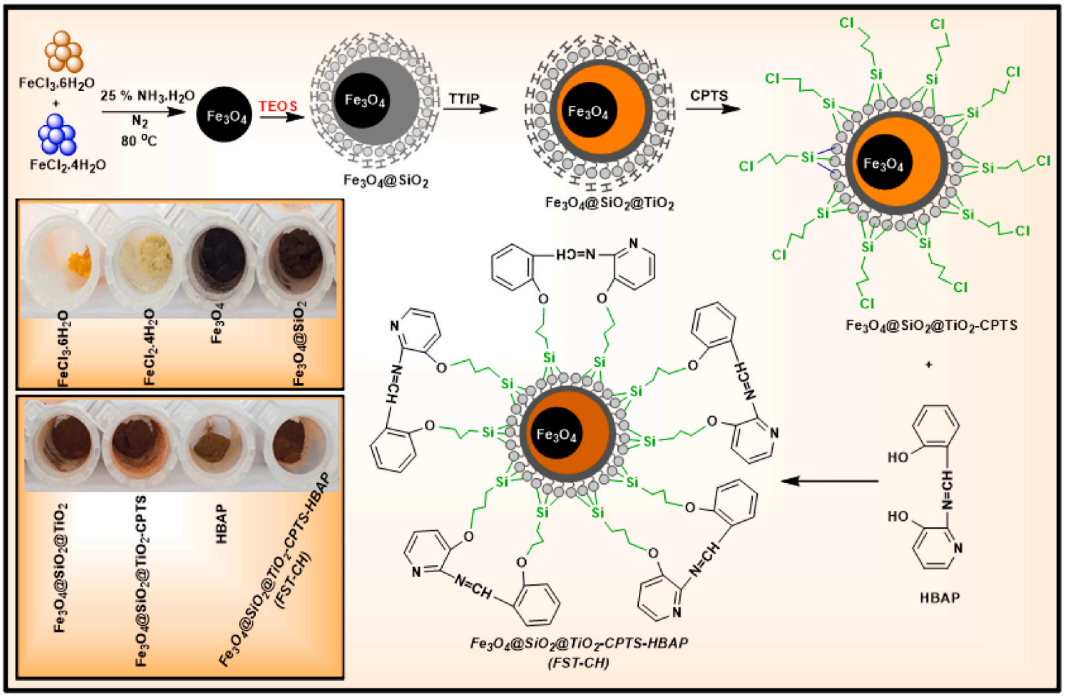

Fig. 1. Schematic illustration for the synthesis of magnetic **$Fe_3O_4@SiO_2@TiO_2$-CPTS-HBAP (FST-CH)** nanoparticles.

(E)-2-((2-hydroxybenzylidene)amino)pyridin-3-ol (HBAP) compound and the photocatalytic degradation of the functional catalyst RhB. Therefore, in the related study, magnetic **Fe_3O_4@SiO_2@TiO_2-CPTS-HBAP (FST-CH)** nanoparticles were synthesized for the isochronous adsorption and photocatalytic degradation of RhB. The synthesis procedure and application scheme of magnetic FST-CH nanoparticles are shown in Fig. 1 in detail. The prepared magnetic nanoparticle is multifunctional and can realize isochronous adsorption and photocatalytic degradation of RhB in UV light. The outcomes demonstrated that about 56% of RhB was adsorbed by the magnetic ***FST-CH*** nanoparticles with only 45 min of stirring, and about 77.01% of RhB was converted after 120 min of UV light. Photocatalytic degradation chased the pseudo second order (PSO) reaction with an apparent rate constant of 0.0026 mg dm^{-3} min^{-1}. Even after four treatments, the synthesized magnetic nanoparticle was sufficiently stable and achieved a normal degradation rate and catalyst recovery. On the other hand, it was observed that the photocatalytic activity of ***FST-CH*** nanoparticles did not increase sufficiently. This is because when organic material is attached to the surface of Fe_3O_4@SiO_2@TiO_2 materials, it does not increase the photocatalytic activity at the desired level. However, it fully demonstrates the potential applications of FST-CH nanoparticles in environmental remediation, and it is thought that this study will also guide the removal of dyes such as rhodamine B and other pollutants from the environment in future studies.

2. Experimental section

2.1. Chemicals and devices

Triethylamine (TEA), hydrochloric acid (37%), ammonium hydroxide solution (25%), $FeCl_2.4H_2O$ (iron(II) chloride tetra hydrate, 99%), $FeCl_3.6H_2O$ (iron (III) chloride hexahydrate, 99%), ethanol (99%), toluene (99.8%), sodium hydroxide (≥98%), acetone (99.5%), andtetraethyl orthosilicate (TEOS, ≥99.0 %) were buyed from Merck (Darmstadt/Germany). Tetrabutyl titanate (TBOT), methanol (HPLC-grade, ≥99.9%), rhodamine B, 1,8-bis (3-chloropropoxy) anthracene-9,10-dione (CPA), isopropyl alcohol ((2-propanol) ≥99.7%), 3-(Chloropropyl)-trimethoxysilane ($Cl(CH_2)_3Si(OCH_3)_3$ (CPTS) and Assay (GC, area%): ≥98.0% (a/a)), and molecular sieves (4 Å beads 8–12 mesh) were buyed from Sigma Aldrich Co. (USA). Unless otherwise stated, all of the compounds used in the study were of analytical grade and no further purification was done. FTIR spectra used in the characterization of nanoparticles synthesized at each stage were recorded within an intensity range of (400–4000 cm^{-1}) on FTIR measure equipment (FTIR, Bruker Vertex 70 ATRFTIR). Scanning electron microscopy (SEM) images and the energy dispersive X-Ray (EDX) analysis were determined with SEM-EDX ((HITACHI (SU5000)). With the Kerman UV 8/18 reactor, photocatalytic studies were conducted.With the aid of a benchtop pH meter (Jenway 3010 digital), pH studies in photocatalytic degradation experiments were adjusted.

2.2. Synthesis of Fe_3O_4 nanoparticles

The Fe_3O_4 were prepared by the previously widely used co-precipitation (CPT) method [41]. Firstly, 9.4 g of anhydrous $FeCl_3$, 5.4 g of $FeCl_2.4H_2O$, and 200 mL of distilled water were added to the reaction vessel and stirred vigorously (at 850 rpm) for 30 min under N_2 atmosphere. At the end of this period, the temperature was increased to 80 °C at reflux at certain time intervals, and 20 mL of $NH_3.H_2O$ (25%) was added dropwise to this mixture and stirred vigorously for another 60 min. Fe_3O_4 nanoparticles in the suspension solution were separated by a magnet and washed with copious amounts of ethanol and deionized water. The nanoparticles were then kept in an oven at 80 °C for one day to be ready for SiO_2 coating.The general procedure of Fe_3O_4 nanoparticles prepared by the coprecipitation method is given in Fig. 1.

2.3. Synthesis of Fe_3O_4@SiO_2 nanoparticles

The surface of the prepared Fe_3O_4 nanoparticles was covered with a SiO_2 shell by applying the Stöber method used in similar studies [42–44]. 0.5 g Fe_3O_4 were added to a 500 mL reaction bowl founding 50 mL of distilled water and 200 mL of ethanol and sonicated for 45 min under ambient conditions [45]. After sonication, 5 mL of 25% NH_3H_2O was added to the suspension solution and stirred vigorously (700 rpm) at room temperature [43]. Then, 3 mL of tetraethyl orthosilicate (TEOS) was added and this suspension solution was stirred in a mechanical mixer (800 rpm) at room temperature (24 h). Fe_3O_4@SiO_2 in the suspension solution were separated with a magnet, they were washed with ethanol and deionized water. It was then dried in furnace at 70 °C overnight. The possible general procedure of Fe_3O_4@SiO_2 prepared by the Stöber method is given in Fig. 1.

2.4. Synthesis of Fe_3O_4@SiO_2@TiO_2nanoparticles

The preparation of Fe_3O_4@SiO_2@TiO_2 nanoparticles was carried out similarly to previous studies [46,47]. After Fe_3O_4 @SiO_2 were synthesized, they were added to the reaction bowl containing 40 mL of ethanol (98%) and sonicated for 30 min. Then, 0.20 mL of deionized water and 1 mL of tetrabutyl titanate (TBOT) were added to this reaction vessel, and the resulting suspension was sonicated for 3 h. Then, the Fe_3O_4@SiO_2@TiO_2 nanoparticles in the mixture were separated with the help of a magnet and washed with ethanol several times. Then, Fe_3O_4@SiO_2@TiO_2 were dried and calcined at 500 °C for 3 h. The probable general procedure of the prepared Fe_3O_4@SiO_2@TiO_2 nanoparticles is given in Fig. 1.

2.5. Synthesis of Fe_3O_4@SiO_2@TiO_2-CPTS nanoparticles

Fe_3O_4@SiO_2@TiO_2 and toluene were added to the reaction vessel and sonicated for 30 min 3-(Chloropropyl)-trimethoxysilane (CPTS) was then added and refluxed at 110 °C for 72 h. After this process was completed, Fe_3O_4@SiO_2@TiO_2-CPTS in the mixture was separated with an magnet, washed with toluene and ethanol and dried at 70 °C for 24 h. Fe_3O_4@SiO_2@TiO_2-CPTS are given in Fig. 1.

2.6. Synthesis of **Fe_3O_4@SiO_2@TiO_2-CPTS-HBAP(FST-CH)** nanoparticles

After adding Fe_3O_4@SiO_2@TiO_2-CPTS and 0.2 g HBAP to the reaction vessel containing 60 mL of anhydrous toluene, 0.1 mL of triethylamine was added to this mixture. It was then stirred under reflux for 72 h at 110 °C. After the process was completed, the solid phase was magnetized and washed with toluene-ethanol (1:1) and dried at 70 °C for 24 h. The probable structure of the obtained **Fe_3O_4@SiO_2@TiO_2-CPTS-HBAP** (**FST-CH**) nanoparticle is shown in Fig. 1.

2.7. Photocatalytic activity experiments

The degradation of RhB dye was researched to calculate the photoactivity of magnetic ***FST-CH*** nanoparticles. Photocatalytic activity studies were carried out using a UV 8/18 vertical cylinder photocatalytic reactor (Kerman). Studies contain 50 mL of 10 mg/LRhB and 0.5 g/L catalyst (***FST-CH***) in a 100 mL beaker at room temperature. To ensure an equilibrium between the photocatalyst and dye for adsorption-desorption, the suspension was continuously stirred for about 45 min in the dark. Then the mixture was placed in Kerman UV 8/18 vertical cylinder photoreactor under magnetic stirring. During the illumination, samples of the mixture were taken at predetermined intervals (15-30-45-60-75-90-105 and 120 min). Then the samples were separated with the help of an externally applied magnet and analyzed with the UV–vis spectrometer(RhB at 555 nm). The obtained data were calculated according to the photocatalytic degradation percentage equation (1) given below.

Degradation percent

$$(\%) = ((C_0\text{-}Ct) / C_0) \text{ x } 100 \quad (1)$$

where C_0 and C_t are the initial concentration of the solution and concentration of the solution at t min, respectively. Aqueous solutions of 0.1 mol L^{-1} each of hydrochloric acid and Sodium hydroxide were used to adjust the pH of the RhB dye solution.

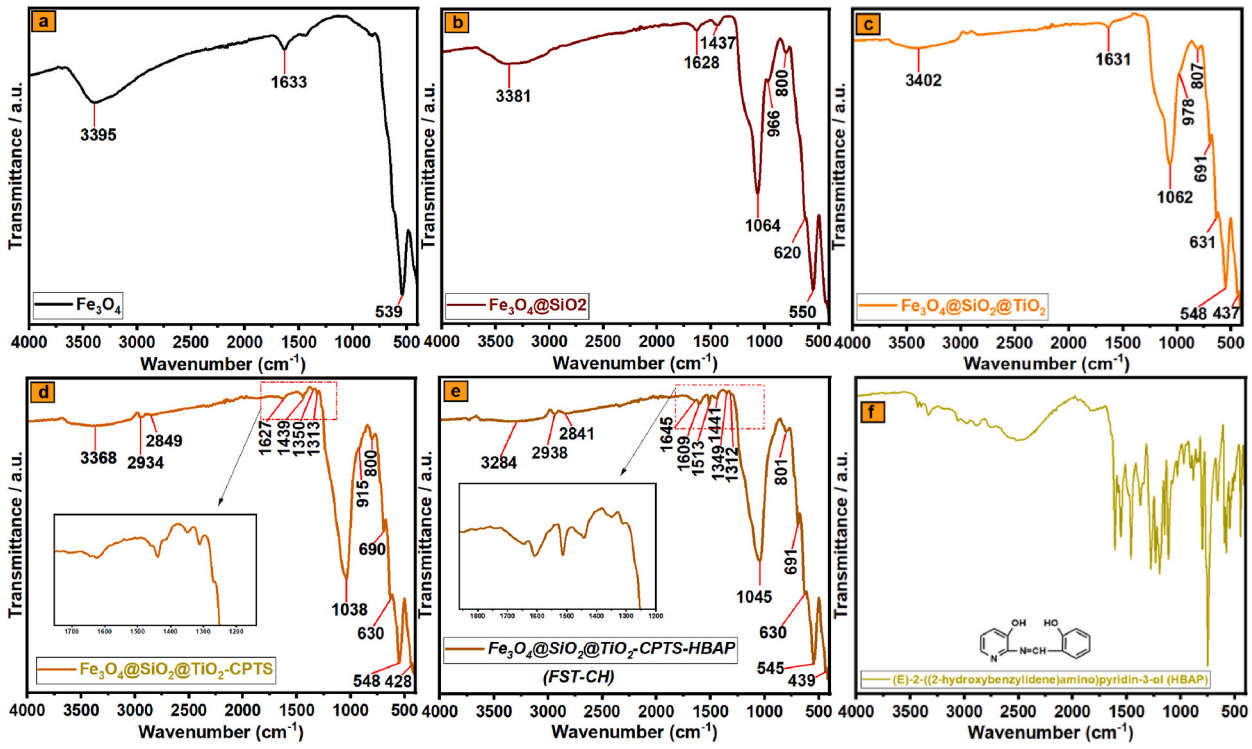

Fig. 2. The FT-IR spectra of **(a)** Fe_3O_4, **(b)** Fe_3O_4@SiO_2, (c) Fe_3O_4@SiO_2@TiO_2**(d)** Fe_3O_4@SiO_2@TiO_2-CPTS, **(e)** ***FST-CH*** nanoparticle and **(f)** HBAP compound.

3. Results and discussions

3.1. Characterizations

3.1.1. FTIR analysis

Each synthesized nanoparticle was analyzed by FTIR and the results obtained in the range of 4000-400 cm^{-1} are shown in Fig. 2a-e. In the Fe_3O_4 nanoparticle shown in Fig. 2a, the broad peak at 3395 cm-1 represents the O–H stretching vibration [48–51]. Also, the peaks at 539 cm^{-1} and 1633 cm^{-1} represent the vibration band of the Fe–O bond and the vibrations of water molecules adsorbed on the nanoparticle surface, respectively [43,50–53]. It is seen that new peaks are formed at 800 cm^{-1}, 966 cm^{-1} and 1064 cm^{-1} in Fe_3O_4@SiO_2 nanoparticle (Fig. 2b). The peak at 966 cm^{-1} represents the bending vibration of Si–OH [50,54]. The absorption peaks at 800 $cm^{-1}$and 1064 cm^{-1} represent the symmetric and asymmetric stretching vibrations of Si–*O*–Si, respectively [49–51,55,56]. These new peaks show that SiO_2 is successfully coated onto of Fe_3O_4 surface. Several new peaks were observed in the FTIR spectrum of the Fe_3O_4@SiO_2@TiO_2 nanoparticle shown in Fig. 2c. It is stated that these peaks are the approximate stretching vibration peaks of Ti–*O*–Ti (437 cm^{-1} and 691 cm^{-1}) [57–59].The absorption peak at around 978 cm^{-1} represents the vibration of Si–O–Ti [50,51,60]. The broad absorption band in the 3402 cm^{-1} represents the Ti–OH groups [61].Several new peaks were observed in the FTIR spectrum of Fe_3O_4@SiO_2@TiO_2-CPTS nanoparticle (Fig. 2d), which is formed as a result of the bonding of the CPTS on the surface of Fe_3O_4@SiO_2@TiO_2 nanoparticle. As seen in Fig. 2d, the weak peaks around 1439 cm^{-1} and 2934-2849 cm^{-1} are related to Si–CH_2 and CH_2 stretching vibrations, respectively.These and other new peaks, and shifts in the peaks confirm the successful binding of the CPTS to

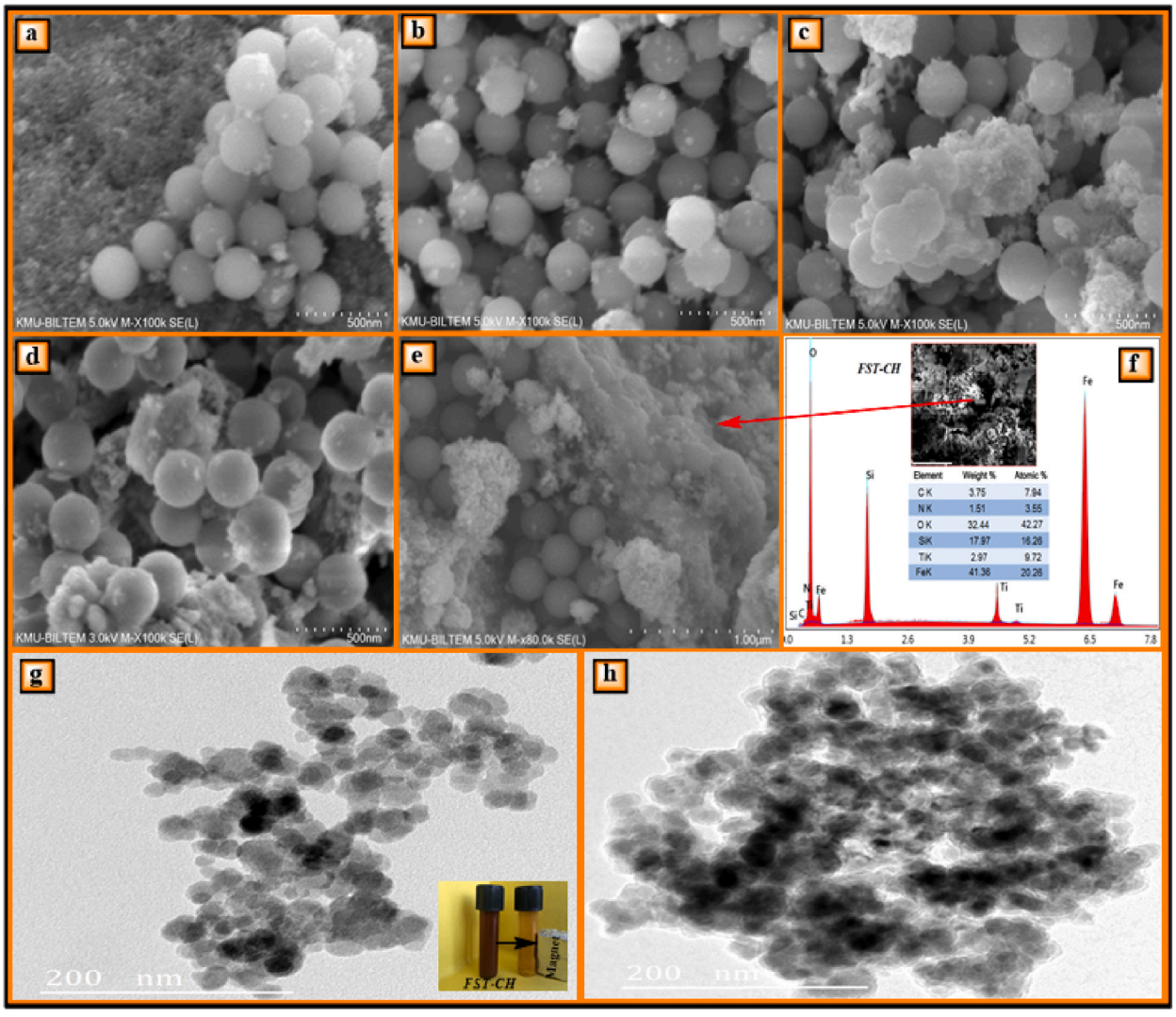

Fig. 3. SEM images of **(a)** Fe_3O_4, **(b)** Fe_3O_4@SiO_2, (c) Fe_3O_4@SiO_2@TiO_2, **(d)** Fe_3O_4@SiO_2@TiO_2-CPTS, **(e)** ***FST-CH*** nanoparticle, **(f)** EDX analysis of ***FST-CH*** nanoparticle, TEM images of **(g)** Fe_3O_4 and **(h)** ***FST-CH*** nanoparticle.

the nanoparticle surface.The new peaks appearing in the FT-IR spectrum of the magnetic **Fe_3O_4@SiO_2@TiO_2-CPTS-HBAP (FST-CH)** nanoparticle in Fig. 2e, at 1645 cm^{-1} (C═N group) and 1513–1609 cm^{-1} (C═C in aromatic rings) indicate the formation of HBAP. Other novel peaks and shifts in the FTIR spectrum of the ***FST-CH*** nanoparticle in Fig. 2e confirm the successful binding of the HBAP to the nanoparticle surface. The FTIR spectrum of the HBAP is given in Fig. 2f.

3.1.2. SEM, EDX and TEM analysis

The morphological structure of the nanoparticles prepared at each stage was evaluated by SEM and SEM images are given in Fig. 3a–e. As seen in the SEM images (Fig. 3a–e), there are generally large/small-sized nanoparticles and the focus was on large spheres in the SEM images. The nanoparticles in Fig. 3a (Fe_3O_4), Fig. 3b (Fe_3O_4/SiO_2), and Fig. 3c (Fe_3O_4@SiO_2@TiO_2) have a spherical structure with average diameters of approximately 210 nm, 215 nm, and 220 nm, respectively. It is seen that TiO_2 is coated very thinly on the Fe_3O_4/SiO_2 surface. Fe_3O_4@SiO_2@TiO_2-CPTS (Fig. 3d) and ***FST-CH*** (Fig. 3e) nanoparticles also exhibited spherical structures with average diameters of about 224 nm and 230 nm, respectively. From the SEM images (Fig. 3a–e), it can be noticed that the size of the spheres increased due to the coating layer. EDX analysis was performed to provide information about the purity of the ***FST-CH*** nanoparticle and the EDX analysis result obtained is given in Fig. 3f. EDX analysis of the ***FST-CH*** nanoparticle confirmed the presence of C, N, O, Fe, Si, and Ti elements (inner Table in Fig. 3f). The very weak Ti peak (2.97 % by weightinner Table in Fig. 3f) in the EDX analysis, shows that little coating of TiO_2 on the surface of the ***FST-CH*** nanoparticle. These EDX results showed that a high-purity nanocomposite of ***FST-CH*** nanoparticle was obtained.

TEM analysis of Fe_3O_4 and FST-CH nanoparticles was performed and the results are shown in Fig. 3g and h. As seen in the TEM results of the prepared Fe_3O_4 particles (Fig. 3g), it is seen that the iron oxide nanoparticles are spherical in form and homogeneously dispersed. The particle size distribution analysis of the prepared Fe_3O_4 nanoparticle was performed and it was determined that it had diameters in the range of 120–270 nm and an average diameter of 212 nm. On the other hand, as seen in the TEM analysis of the synthesized ***FST-CH*** nanoparticle (Fig. 3h), it shows that due to the amorphous structure of SiO_2, it is coated on the surface of Fe_3O_4 as a thinner flat layer. On the surface of Fe_3O_4@SiO_2 nanoparticle, which have a spherical shape, TiO_2 was heterogeneously dispersed and the heterogeneous distribution formed malformation. As a result of the particle size distribution analysis for ***FST-CH*** nanoparticles, it was determined that the nanoparticles had diameters ranging from 140 to 295 nm and an average diameter of around 245 nm.

3.1.3. XRD analysis

To investigate the chemical structure and phase of the nanocomposite, X-ray diffraction of the nanoparticles prepared for each step was performed and the XRD spectra obtained are given in Fig. 4a–d. The detectioned peaks in 2θ of 30.3°(220), 35.9°(311), 43.1°(400), 57.4°(511), and 62.7°(440) for Fe_3O_4 complatelly compatible with the standard XRD spectral data (Fig. 4a) [34,49,62]. The XRD model (Fig. 4b) of Fe_3O4@SiO_2 nanoparticles formed after SiO2 coating on the surface of Fe_3O_4 magnetic nanoparticles appears to have the same diffraction peak as Fe_3O_4, which means that the crystal structure of Fe_3O_4 is preserved after SiO_2 coating [62]. The XRD spectrum of the Fe_3O_4@SiO_2@TiO_2 (FST) in Fig. 4c confirmed a serial of diffraction peaks at locations 25.30° (101), 37.13°(004), and 48.17° (200) was in accordance with the registered data of TiO_2 (JCPDS card no. 21–1272) [63]. In 2-theta, peaks related to TiO_2 appear to be small at 25.30°, 37.13°, and 48.17°. As stated in other studies, the reason why the titanium diffraction peaks cannot be seen clearly may be due to the very thinness of the titanium shell [34,50]. The ***FST-CH*** nanoparticle XRD model (Fig. 4d) shows that the peaks of the FST are the same and the density of these peaks raise or decrease and widen or narrow.

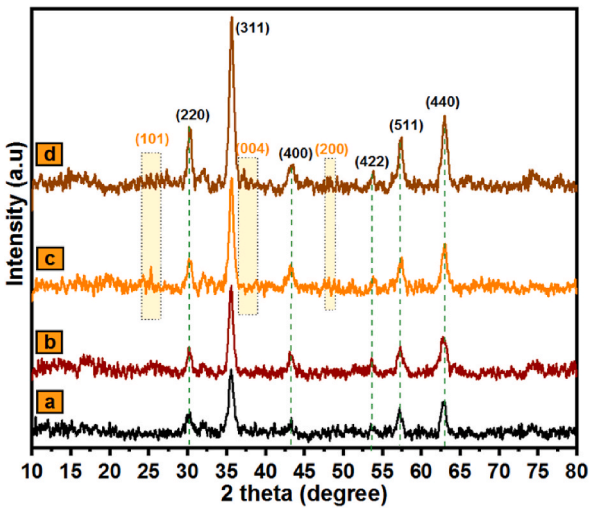

Fig. 4. XRD spectra of**(a)** Fe_3O_4, **(b)** Fe_3O_4@SiO_2, (c) Fe_3O_4@SiO_2@TiO_2, and **(d)** ***FST-CH*** nanoparticle.

3.2. Photocatalytic activity

Photocatalytic activities of Fe_3O_4@SiO_2@TiO_2 and ***FST-CH*** were evaluated by photocatalytic degradation of RhB in aqueous solution with the aid of a photoreactor (Kerman UV 8/18 vertical cylinder). In dark conditions (about 30 min) on the surface of the catalysts, the adsorption-desorption equilibrium of RhB is established. TiO_2-based materials or all other catalysts have similar adsorption capability in the range of 4–15% Ct/C0 of RhB in the aqueous medium [64–66]. Also, illumination in the absence of all catalysts such as Fe_3O_4@SiO_2@$TiO_2$and ***FST-CH*** nanoparticles does not result in photocatalytic decolorization of RhB [31]. As a result, for the efficient deterioration to occur effectively of RhB, both UV irradiation and materials made TiO_2-based are required. The absorption peak of the RhB dye at 555 nm in the UV–vis spectrometer was chosen to study the photocatalytic degradation period. The change of RhB dye concentration during the photodegradation process of Fe_3O_4@SiO_2@TiO_2 and ***FST-CH*** nanoparticles is shown in Fig. 5a. As seen in Fig. 5a, the RhB dye concentration decreases significantly after ***FST-CH*** and RhB are mixed for 45 min in the dark. It is seen that approximately 56% of the RhB molecules are adsorbed on the ***FST-CH*** nanoparticle hybrids by mixing for only 45 min in the dark environment reaction (Fig. 5b). On the other hand, under the irradiation of UV light, the RhB concentration appears to decrease continuously to about 2.92% with an irradiation time of up to 120 min (Fig. 5a). This suggests that 77.01% of RhB can progressively degrade or transform into other structures in the presence of ***FST-CH*** nanoparticles under UV light irradiation. However, for Fe_3O_4@SiO_2@TiO_2, 13.18% (Fig. 5a) of RhB molecules in the dark environment reaction appears to be adsorbed on Fe_3O_4@SiO_2@TiO_2nanoparticles. In the presence of Fe_3O_4@SiO_2@TiO_2nanoparticles, 69.77% of RhB can be progressively degraded or converted to other structures, with an irradiation time of up to 120 min. All of these indicate that the prepared ***FST-CH*** nanoparticles have the ability to adsorb aromatic compounds through π–π stowing and other molecular interactions, and also have good a photocatalytic activity.

Pseudo-first-order (PFO) and pseudo-second-order (PSO) kinetic models, which are widely used in many studies, were used to examine the photocatalytic degradation kinetics of RhB. The linear forms of these kinetic models are given in Table 1. Where C0, Ct, represent the initial concentration of RhB (mg dm^{-3}) and the concentration of RhB at time t (min) (mg dm^{-3}), respectively. The same time k_1 ve k_2 represent PFO decay rate constant and the PSO the degradation rate constant (mg dm-3 min-1), respectively [58]. According to the equation of the PFO kinetic model in Table 1, PFO decay rate constant (k_1) was calculated by plotting the linear regression of irradiation time (t) versus -ln(C_t/C_0) (Fig. 6a). The k_1 and R^2 values obtained from this graph (Fig. 6a) are given in Table 1. According to the equation of the PSO kinetic model in Table 1, the quadratic decay rate constant (k_2) was calculated by the slope of the straight line obtained by plotting the $1/C_t$ - $1/C_0$ linear regression against irradiation time (t) (Fig. 6b). The k_2 and R^2 values obtained from this graph (Fig. 6b) are given in Table 1.

As seen in Table 1, for Fe_3O_4@SiO_2@TiO_2 nanoparticles, for the PFO model, the linear correlation coefficient ($R^2 = 0.9572$) is greater than the PSO correlation coefficient ($R^2 = 0.9902$). An exponential fall of RhB dye concentration with irradiation time is evident, indicating that the RhB photodegradation process by Fe_3O_4@SiO_2@TiO_2 follows a PFO reaction. On the other hand, for ***FST-CH*** nanoparticles, It can be seen (Table 1) that for the PFO model, the linear correlation coefficient ($R^2 = 0.9781$) was lower than the PSO correlation coefficient ($R^2 = 0.987$). The rate constant (k_2) of ***FST-CH*** nanoparticles is 0.0026 mg dm^{-3} min^{-1}, and the rate constant (k_2) found for Fe_3O_4@SiO_2@TiO_2 is slightly higher at 0.002 mg dm^{-3} min^{-1}. According to the obtained data, the photocatalytic degradation of RhB by the ***FST-CH*** nanoparticles was best fitted with PSO kinetics and the synthesized ***FST-CH*** nanoparticles indicate good catalytic activity. An amphoteric dye is rhodamine B. There are both negatively and positively charged groups on the molecule [67]. It is thought that the reason why Fe_3O_4@SiO_2@TiO_2 and ***FST-CH*** show compatibility with different kinetic models in

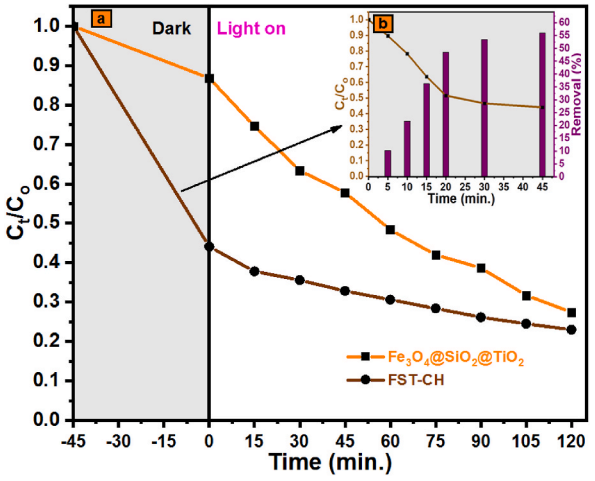

Fig. 5. **(a)** Fe_3O_4@SiO_2@TiO_2 and ***FST-CH*** nanoparticles change of RhB dye concentration as a function of irradiation time in the dark and under lamp irradiation (They were kept in the dark for 45 min and the light exposure time was set to 0) and **(b)** The change in RhB dye adsorption concentration and removal (%) (0–45 min)of ***FST-CH*** nanoparticles in the dark environment.(Experimental Conditions = pH: 8.0, Temperature 25 °C, ***FST-CH*** nanoparticles dose: 0.5 g/L,and RhB concentration: 10 μM).

Table 1
The reaction rate constant for the PFO and PSO kinetic of RhB photocatalytic degradation by Fe_3O_4@SiO_2@$TiO_2$and ***FST-CH*** nanoparticles.

	The kinetic models					
	The pseudo-first-order (PFO)		Ref.	**The pseudo-second-order (PSO)**		Ref.
	$\ln C_0/C_t = k_1 \cdot t$		[68]	$1/C_t - 1/C_0 = k_2 \cdot t$		[68]
	R^2	$k_1(min^{-1})$		R^2	$k_2(mg\ dm^{-3}\ min^{-1})$	
Fe_3O_4@SiO_2@TiO_2	0.9902	0.0089		0.9572	0.002	
FST-CH	0.9781	0.0047		0.987	0.0026	

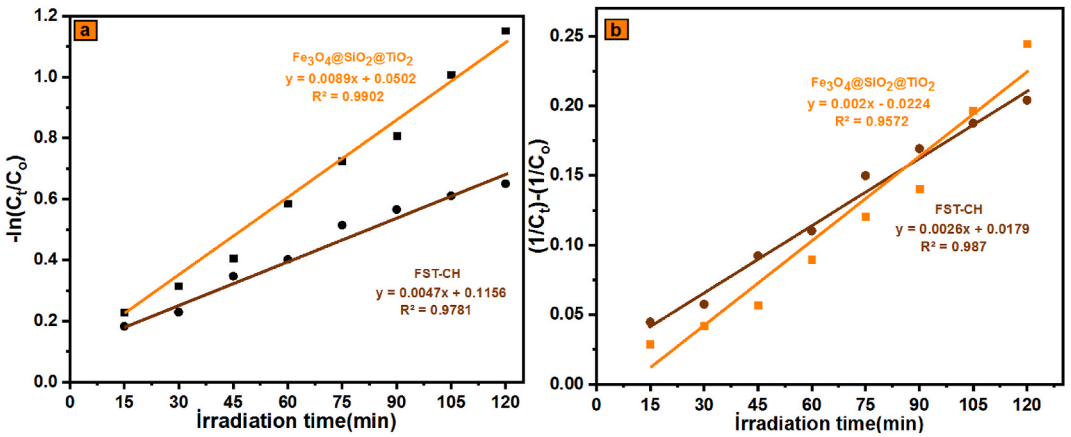

Fig. 6. The PFO plot **(a)** and the PSO plot **(b)** of RhB photocatalytic degradation by Fe_3O_4@SiO_2@TiO_2 and ***FST-CH*** nanoparticles.

the photocatalytic degradation of rhodamine B is because it is an amphoteric dye.

Another important factor is the stability and reusability of the catalyst. For reuse, the prepared ***FST-CH*** nanoparticles were separated from the reaction solution with the help of an external magnet, washed and dried and reused in the next cycle. Four cycles (Fig. 7) were performed. As shown in Fig. 7, after four cycles (photocatalytic degradation of four cycles), the photodegradation efficiency of RhB decreased from 77.01 (1st cycle) to 72.85% (4th cycle). The degradation efficiency over these four cycles stays above 72% during each cycle, which means the catalyst maintains coherent activity. This shows that magnetic FST-CH nanoparticles can work as a durable catalyst in microwave induced dye oxidation and have high stability and favorable reusability under UV light irradiation.

4. Conclusions

Fe_3O_4 nanoparticles were successfully synthesized using the commonly used coprecipitation technique. Fe3O4@SiO2@TiO2 was prepared by the typical Stöber method and Fe_3O_4@SiO_2@TiO_2 was obtained by the sol-gel technique. The magnetic ***FST-CH*** nanoparticles were successfully prepared as a result of the modification of the CPTS compound and the immobilization of the HBAP compound on the surface of Fe_3O_4@SiO_2@TiO_2. The samples were evaluated by XRD, FTIR, SEM, and EDX techniques. It has been shown that the prepared ***FST-CH*** nanoparticles have an excellent adsorbing ability toward RhB aromatic compounds through molecular interactions. The magnetic Fe_3O_4 in the core of the prepared ***FST-CH*** nanoparticles facilitated the separation of the ***FST-CH*** nanoparticles from the solution with the help of an magnet, and the titania stratum acted as a photocatalyst to decompose the RhB from water. Photocatalytic experiments carried out indicate that the magnetic FST-CH nanoparticles show good a photocatalytic activitie under UV light and can be reused at least four times with almost unaffected photocatalytic efficiency, pointing to its potential application in water purification.

CRediT authorship contribution statement

Aysel Cimen: Writing – review & editing, Writing – original draft, Visualization, Validation, Supervision, Software, Resources, Project administration, Methodology, Investigation, Funding acquisition, Formal analysis, Data curation, Conceptualization. **Ali Bilgic:** Writing – review & editing, Visualization, Software, Resources, Methodology, Formal analysis, Data curation. **Melike Bayrak:** Data curation.

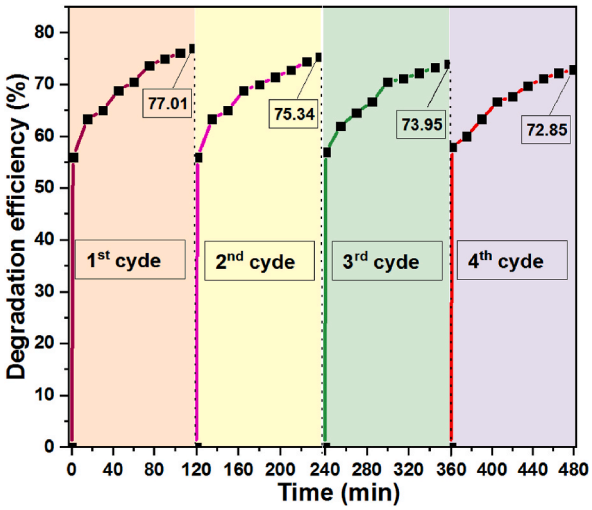

Fig. 7. Reusability efficiencies of***FST-CH***nanoparticles for four consecutive cycles.

Declaration of competing interest

The authors of this article declare that they have no competing financial interests or personal relationships that could affect the work reported in the article.

Acknowledgments

The authors of this article would like to thank Karamanoğlu Mehmetbey University Scientific Research Project Commission for their financial support (BAP-Grant no 13-*M*-21).

References

[1] P. Nandigana, S. Mahato, M. Dhandapani, B. Pradhan, B. Subramanian, S.K. Panda, Lyophilized tin-doped MoS2 as an efficient photocatalyst for overall degradation of Rhodamine B dye, J. Alloys Compd. 907 (2022) 164470.
[2] D. Zhang, G. Li, C.Y. Jimmy, Inorganic materials for photocatalytic water disinfection, J. Mater. Chem. 20 (22) (2010) 4529–4536.
[3] F. Ghasemy-Piranloo, S. Dadashian, F. Bavarsiha, Fe3O4/SiO2/TiO2–Ag cubes with core/shell/shell nano-structure: synthesis, characterization and efficient photo-catalytic for phenol degradation, J. Mater. Sci. Mater. Electron. 30 (13) (2019) 12757–12768.
[4] T. Varadavenkatesan, E. Lyubchik, S. Pai, A. Pugazhendhi, R. Vinayagam, R. Selvaraj, Photocatalytic degradation of Rhodamine B by zinc oxide nanoparticles synthesized using the leaf extract of Cyanometra ramiflora, J. Photochem. Photobiol. B Biol. 199 (2019) 111621.
[5] X. Liu, K. Chen, J.-J. Shim, J. Huang, Facile synthesis of porous Fe2O3 nanorods and their photocatalytic properties, J. Saudi Chem. Soc. 19 (5) (2015) 479–484.
[6] M. Ahmad, W. Rehman, M.M. Khan, M.T. Qureshi, A. Gul, S. Haq, R. Ullah, A. Rab, F. Menaa, Phytogenic fabrication of ZnO and gold decorated ZnO nanoparticles for photocatalytic degradation of Rhodamine B, J. Environ. Chem. Eng. 9 (1) (2021) 104725.
[7] Q. Wang, S.M. Shaheen, Y. Jiang, R. Li, M. Slaný, H. Abdelrahman, E. Kwon, N. Bolan, J. Rinklebe, Z. Zhang, Fe/Mn-and P-modified drinking water treatment residuals reduced Cu and Pb phytoavailability and uptake in a mining soil, J. Hazard Mater. 403 (2021) 123628.
[8] R. Kumar, J. Rashid, M. Barakat, Zero valent Ag deposited TiO2 for the efficient photocatalysis of methylene blue under UV-C light irradiation, Colloids Interface Sci. Commun. 5 (2015) 1–4.
[9] A.A. Al-Gheethi, Q.M. Azhar, P.S. Kumar, A.A. Yusuf, A.K. Al-Buriahi, R.M.S.R. Mohamed, M.M. Al-Shaibani, Sustainable approaches for removing Rhodamine B dye using agricultural waste adsorbents: a review, Chemosphere 287 (2022) 132080.
[10] C. Lops, A. Ancona, K. Di Cesare, B. Dumontel, N. Garino, G. Canavese, S. Hérnandez, V. Cauda, Sonophotocatalytic degradation mechanisms of Rhodamine B dye via radicals generation by micro-and nano-particles of ZnO, Appl. Catal. B Environ. 243 (2019) 629–640.
[11] S. Merouani, O. Hamdaoui, F. Saoudi, M. Chiha, Sonochemical degradation of Rhodamine B in aqueous phase: effects of additives, Chem. Eng. J. 158 (3) (2010) 550–557.
[12] N. Madima, K.K. Kefeni, S.B. Mishra, A.K. Mishra, A.T. Kuvarega, Fabrication of magnetic recoverable Fe3O4/TiO2 heterostructure for photocatalytic degradation of rhodamine B dye, Inorg. Chem. Commun. 145 (2022) 109966.
[13] U.G. Akpan, B.H. Hameed, Parameters affecting the photocatalytic degradation of dyes using TiO2-based photocatalysts: a review, J. Hazard Mater. 170 (2–3) (2009) 520–529.
[14] S.G. Schrank, J.N.R. Dos Santos, D.S. Souza, E.E.S. Souza, Decolourisation effects of Vat Green 01 textile dye and textile wastewater using H2O2/UV process, J. Photochem. Photobiol. A Chemistry 186 (2–3) (2007) 125–129.
[15] T. Zhao, P. Li, C. Tai, J. She, Y. Yin, G. Zhang, Efficient decolorization of typical azo dyes using low-frequency ultrasound in presence of carbonate and hydrogen peroxide, J. Hazard Mater. 346 (2018) 42–51.
[16] I.H. Chowdhury, S. Kundu, M.K. Naskar, Template-free hydrothermal synthesis of MgO-TiO2 microcubes toward high potential removal of toxic water pollutants, J. Phys. Chem. Solid. 112 (2018) 171–178.
[17] K. Kaur, R. Badru, P.P. Singh, S. Kaushal, Photodegradation of organic pollutants using heterojunctions: a review, J. Environ. Chem. Eng. 8 (2) (2020) 103666.
[18] M. Ranjeh, F. Beshkar, O. Amiri, M. Salavati-Niasari, H. Moayedi, Pechini sol-gel synthesis of Cu2O/Li3BO3 and CuO/Li3BO3 nanocomposites for visible light-driven photocatalytic degradation of dye pollutant, J. Alloys Compd. 815 (2020) 152451.
[19] H.A. Alshamsi, F. Beshkar, O. Amiri, M. Salavati-Niasari, Porous hollow Ag/Ag2S/Ag3PO4 nanocomposites as highly efficient heterojunction photocatalysts for the removal of antibiotics under simulated sunlight irradiation, Chemosphere 274 (2021) 129765.

[20] H. Suzuki, S. Araki, H. Yamamoto, Evaluation of advanced oxidation processes (AOP) using O3, UV, and TiO2 for the degradation of phenol in water, J. Water Process Eng. 7 (2015) 54–60.
[21] E. Mrotek, S. Dudziak, I. Malinowska, D. Pelczarski, Z. Ryżyńska, A. Zielińska-Jurek, Improved degradation of etodolac in the presence of core-shell ZnFe2O4/SiO2/TiO2 magnetic photocatalyst, Sci. Total Environ. 724 (2020) 138167.
[22] P.L. Hariani, M. Said, N. Aprianti, Y.A.L.R. Naibaho, High efficient photocatalytic degradation of methyl orange dye in an aqueous solution by CoFe2O4-SiO2-TiO2 magnetic catalyst, J. Ecol. Eng. 23 (1) (2022).
[23] A. Takdastan, B. Kakavandi, M. Azizi, M. Golshan, Efficient activation of peroxymonosulfate by using ferroferric oxide supported on carbon/UV/US system: a new approach into catalytic degradation of bisphenol A, Chem. Eng. J. 331 (2018) 729–743.
[24] J. Ge, Y. Zhang, Y.-J. Heo, S.-J. Park, Advanced design and synthesis of composite photocatalysts for the remediation of wastewater: a review, Catalysts 9 (2) (2019) 122.
[25] D. Beketova, M. Motola, H. Sopha, J. Michalicka, V. Cicmancova, F. Dvorak, L. Hromadko, B. Frumarova, M. Stoica, J.M. Macak, One-step decoration of TiO2 nanotubes with Fe3O4 nanoparticles: synthesis and photocatalytic and magnetic properties, ACS Appl. Nano Mater. 3 (2) (2020) 1553–1563.
[26] D. Manoj, S. Rajendran, Y. Vasseghian, S. Ansar, F. Gracia, M. Soto-Moscoso, Tailoring the heterojunction of TiO2 with multivalence CeO2 nanocrystals-for detection of toxic 2-aminophenol, Food Chem. Toxicol. (2022) 113182.
[27] B. Ohtani, Photocatalysis A to Z—what we know and what we do not know in a scientific sense, J. Photochem. Photobiol., A 11 (4) (2010) 157–178.
[28] S.-A. Lee, K.-H. Choo, C.-H. Lee, H.-I. Lee, T. Hyeon, W. Choi, H.-H. Kwon, Use of ultrafiltration membranes for the separation of TiO2 photocatalysts in drinking water treatment, Ind. Eng. Chem. Res. 40 (7) (2001) 1712–1719.
[29] J. Yuan, Y. Zhang, X. Zhang, L. Zhao, H. Shen, S. Zhang, Template-free synthesis of core—shell Fe3O4@ MoS2@ mesoporous TiO2 magnetic photocatalyst for wastewater treatment, Int. J. Miner. Metall. Mater. 30 (1) (2023) 177–191.
[30] Z.-Y. Chen, W.W.-P. Lai, H.H.-H. Lin, J.X. Tan, K.C.-W. Wu, A.Y.-C. Lin, Photocatalytic degradation of ketamine using a reusable TiO2/SiO2@ Fe3O4 magnetic photocatalyst under simulated solar light, J. Environ. Chem. Eng. 10 (6) (2022) 108637.
[31] F. Chen, F. Yan, Q. Chen, Y. Wang, L. Han, Z. Chen, S. Fang, Fabrication of Fe3O4@SiO2@TiO2 nanoparticles supported by graphene oxide sheets for the repeated adsorption and photocatalytic degradation of rhodamine B under UV irradiation, Dalton trans. 43 (36) (2014) 13537–13544.
[32] P.M. Álvarez, J. Jaramillo, F. Lopez-Pinero, P.K. Plucinski, Preparation and characterization of magnetic TiO2 nanoparticles and their utilization for the degradation of emerging pollutants in water, Appl. Catal. B Environ. 100 (1–2) (2010) 338–345.
[33] M.-P. Mazhari, M. Hamadanian, Preparation and characterization of Fe3O4@ SiO2@ TiO2 and Ag/Fe3O4@ SiO2@ TiO2 nanocomposites for water treatment: process optimization by response surface methodology, J. Electron. Mater. 47 (12) (2018) 7484–7496.
[34] M.A. Habila, Z.A. Alothman, A.M. El-Toni, J.P. Labis, M. Soylak, Synthesis and application of Fe3O4@ SiO2@ TiO2 for photocatalytic decomposition of organic matrix simultaneously with magnetic solid phase extraction of heavy metals prior to ICP-MS analysis, Talanta 154 (2016) 539–547.
[35] F. Absalan, M. Nikazar, Application of response surface methodology for optimization of water treatment by Fe3O4/SiO2/TiO2 core-shell nano-photocatalyst, Chem. Eng. Commun. 203 (11) (2016) 1523–1531.
[36] J. Rashid, M. Barakat, Y. Ruzmanova, A. Chianese, Fe3O4/SiO2/TiO2 nanoparticles for photocatalytic degradation of 2-chlorophenol in simulated wastewater, Environ. Sci. Pollut. Res. 22 (4) (2015) 3149–3157.
[37] H. Liu, Z. Jia, S. Ji, Y. Zheng, M. Li, H. Yang, Synthesis of TiO2/SiO2@Fe3O4 magnetic microspheres and their properties of photocatalytic degradation dyestuff, Catal. Today 175 (1) (2011) 293–298.
[38] S. Behzadi, B. Nonahal, S.J. Royaee, A.A. Asadi, Tio2/SiO2/Fe3O4 magnetic nanoparticles synthesis and application in methyl orange UV photocatalytic removal, Water Sci. Technol. 82 (11) (2020) 2432–2445.
[39] M. Mazhari, A. Abbasi, A. Derakhshan, M. Ahmadi, Fabrication Fe3O4/SiO2/TiO2 nanocomposites and degradation of rhodamine B dyes under UV light irradiation, J Nanostruct 6 (1) (2016) 101–105.
[40] P.L. Hariani, M. Said, A. Rachmat, S. Salni, N. Aprianti, A.F. Amatullah, Catalysis, synthesis of NiFe2O4/SiO2/NiO magnetic and application for the photocatalytic degradation of methyl orange dye under UV irradiation, Bull. Chem. React. Eng. 17 (4) (2022) 699–711.
[41] A. Maleki, T. Kari, M. Aghaei, Fe3O4@ SiO2@ TiO2-OSO3H: an efficient hierarchical nanocatalyst for the organic quinazolines syntheses, J. Porous Mater. 24 (6) (2017) 1481–1496.
[42] W. Stöber, A. Fink, E. Bohn, Controlled growth of monodisperse silica spheres in the micron size range, J. Colloid Interface Sci. 26 (1) (1968) 62–69.
[43] A. Bilgic, A. Cimen, Two novel BODIPY-functional magnetite fluorescent nano-sensors for detecting of Cr (VI) Ions in aqueous solutions, J. Fluoresc. 30 (2020) 867–881.
[44] A. Bilgic, A. Cimen, A highly sensitive and selective ON-OFF fluorescent sensor based on functionalized magnetite nanoparticles for detection of Cr (VI) metal ions in the aqueous medium, J. Mol. Liq. 312 (2020) 113398.
[45] A. Bilgic, A. Cimen, Synthesis, characterization, adsorption studies and comparison of superparamagnetic iron oxide nanoparticles (SPION) with three different amine groups functionalized with BODIPY for the removal of Cr(VI) metal ions from aqueous solutions, Int. J. Environ. Anal. Chem. (2021) 1–26.
[46] E.S. Kunarti, R. Roto, N. Nuryono, S.J. Santosa, M.L. Fajri, Photocatalytic reduction of AuCl4− by Fe3O4/SiO2/TiO2 nanoparticles, Global Nest Journal 22 (1) (2020) 119–125.
[47] F.-M. Pellera, A. Giannis, D. Kalderis, K. Anastasiadou, R. Stegmann, J.-Y. Wang, E. Gidarakos, Adsorption of Cu (II) ions from aqueous solutions on biochars prepared from agricultural by-products, J. Environ. Manag. 96 (1) (2012) 35–42.
[48] R. Thekkathu, D. Ashok, P.K. Ramkollath, S. Neelakandapillai, L.P. Kurishunkal, M.P. Yadav, N. Kalarikkal, Magnetically recoverable Ir/IrO2@ Fe3O4 core/SiO2 shell catalyst for the reduction of organic pollutants in water, Chem. Phys. Lett. 742 (2020) 137147.
[49] A. Bilgiç, H.S. Karapınar, APTMS-BCAD modified magnetic iron oxide for magnetic solid-phase extraction of Cu (II) from aqueous solutions, Heliyon (2022) e09645.
[50] A. Bilgic, Fabrication of monoBODIPY-functionalized Fe3O4@ SiO2@ TiO2 nanoparticles for the photocatalytic degradation of rhodamine B under UV irradiation and the detection and removal of Cu (II) ions in aqueous solutions, J. Alloys Compd. 899 (2022) 163360.
[51] H.S. Karapınar, A. Bilgiç, A new magnetic Fe3O4@SiO2@TiO2-APTMS-CPA adsorbent for simple, fast and effective extraction of aflatoxins from some nuts, J. Food Compos. Anal. 105 (2022) 104261.
[52] T. Kamakshi, G.S. Sundari, H. Erothu, R.S. Singh, Effect of nickel dopant on structural morphological and optical characteristics of Fe3O4 nanoparticles, Rasayan J. Chem. 12 (2) (2019) 531–536.
[53] A. Bilgic, A. Cimen, A highly sensitive and selective ON-OFF fluorescent sensor based on functionalized magnetite nanoparticles for detection of Cr (VI) metal ions in the aqueous medium, J. Mol. Liq. (2020) 113398.
[54] S. Mortazavi-Derazkola, M. Salavati-Niasari, O. Amiri, A. Abbasi, Fabrication and characterization of Fe3O4@SiO2@TiO2@Ho nanostructures as a novel and highly efficient photocatalyst for degradation of organic pollution, J. Energy Chem. 26 (1) (2017) 17–23.
[55] H. Kiziltaş, T. Tekin, D. Tekin, Preparation and characterization of recyclable Fe3O4@SiO2@TiO2 composite photocatalyst, and investigation of the photocatalytic activity, Chem. Eng. Commun. 208 (7) (2021) 1041–1053.
[56] J. Miao, X. Zhao, Y.-X. Zhang, Z.-H. Liu, Feasible synthesis of hierarchical porous MgAl-borate LDHs functionalized Fe3O4@SiO2 magnetic microspheres with excellent adsorption performance toward Congo red and Cr (VI) pollutants, J. Alloys Compd. 861 (2021) 157974.
[57] A.H. Shah, M.A. Rather, Effect of calcination temperature on the crystallite size, particle size and zeta potential of TiO2 nanoparticles synthesized via polyol-mediated method, Mater. Today: Proc. 44 (2021) 482–488.
[58] I. Gabelica, L. Ćurković, V. Mandić, I. Panžić, D. Ljubas, K. Zadro, Rapid microwave-assisted synthesis of Fe3O4/SiO2/TiO2 core-2-layer-shell nanocomposite for photocatalytic degradation of ciprofloxacin, Catalysts 11 (10) (2021) 1136.
[59] M.A. Marsooli, M.R. Nasrabadi, M. Fasihi-Ramandi, K. Adib, M. Eghbali, S. Pourmasoud, F. Ahmadi, E. Sohouli, A.S. Nasab, S.A. Mirhosseini, Preparation of Fe3O4/SiO2/TiO2/PrVO4 nanocomposite in various molar ratios: investigation on photocatalytic performance on organic contaminate and bacterial environments, and anti-cancer properties, Polyhedron 176 (2020) 114239.

[60] Z. Dai, D. Li, L. Chi, Y. Li, B. Gao, N. Qiu, Q. Duan, Y. Li, Preparation of porphyrin sensitized three layers magnetic nanocomposite Fe3O4@SiO2@TiO2 as an efficient photocatalyst, Mater. Lett. 241 (2019) 239–242.
[61] L. Enayati Ahangar, K. Movassaghi, M. Emadi, F. Yaghoobi, Photocatalytic application of TiO2/SiO2-based magnetic nanocomposite (Fe3O4@ SiO2/TiO2) for reusing of textile wastewater, Nano Res. 1 (1) (2016) 33–39.
[62] K.-H. Han, Y.-H. Kim, I.-H. Pak, J.-H. Yu, I.-C. Ho, R.-H. Han, Fe3O4@ SiO2@ TiO2@ PDA nanocomposite for the degradation of organic materials, Chem. Eng. Technol. 45 (1) (2022) 178–188.
[63] J. Li, L. Gao, Q. Zhang, R. Feng, H. Xu, J. Wang, D. Sun, C. Xue, Photocatalytic property of Fe3O4/SiO2/TiO2 core-shell nanoparticle with different functional layer thicknesses, J. Nanomater. 2014 (2014) 2, 2.
[64] Y. Chi, Q. Yuan, Y. Li, L. Zhao, N. Li, X. Li, W. Yan, Magnetically separable Fe3O4@SiO2@TiO2-Ag microspheres with well-designed nanostructure and enhanced photocatalytic activity, J. Hazard Mater. 262 (2013) 404–411.
[65] K.-H. Han, Y.-H. Kim, M.-H. Mun, J.-H. Yu, R.-H. Han, Synthesis of polypyrrole-modified Fe3O4/SiO2/TiO2 nanocomposite microspheres and their photocatalytic activity, Mater. Res. Express 9 (2) (2022) 025007.
[66] X. Li, D. Liu, S. Song, H. Zhang, Fe3O4@ SiO2@ TiO2@ Pt hierarchical core–shell microspheres: controlled synthesis, enhanced degradation system, and rapid magnetic separation to recycle, Cryst. Growth Des. 14 (11) (2014) 5506–5511.
[67] N.A. Jasim, S.E. Ebrahim, S.H. Ammar, Photocatalytic degradation of Rhodamine B using CoxZn1-xFe2O4 nanocomposite under visible light irradiation: synthesis, characterization and its application, Alex. Eng. J. 82 (2023) 557–576.
[68] M. Ahmadi, H.R. Motlagh, N. Jaafarzadeh, A. Mostoufi, R. Saeedi, G. Barzegar, S. Jorfi, Enhanced photocatalytic degradation of tetracycline and real pharmaceutical wastewater using MWCNT/TiO2 nano-composite, J. Environ. Manag. 186 (2017) 55–63.